ARTICLE

doi:10.1038/nature12217

# Anisotropic leaky-mode modulator for holographic video displays

D. E. Smalley[1], Q. Y. J. Smithwick[1], V. M. Bove Jr[1], J. Barabas[1] & S. Jolly[1]

**Every holographic video display is built on a spatial light modulator, which directs light by diffraction to form points in three-dimensional space. The modulators currently used for holographic video displays are challenging to use for several reasons: they have relatively low bandwidth, high cost, low diffraction angle, poor scalability, and the presence of quantization noise, unwanted diffractive orders and zero-order light. Here we present modulators for holographic video displays based on anisotropic leaky-mode couplers, which have the potential to address all of these challenges. These modulators can be fabricated simply, monolithically and at low cost. Additionally, these modulators are capable of new functionalities, such as wavelength division multiplexing for colour display. We demonstrate three enabling properties of particular interest—polarization rotation, enlarged angular diffraction, and frequency domain colour filtering—and suggest that this technology can be used as a platform for low-cost, high-performance holographic video displays.**

The limitations and useful properties (affordances) of holographic video displays are chiefly dictated by the spatial light modulators (SLMs) on which they are built. The temporal bandwidth of the spatial light modulator determines the display size, view angle and frame rate. The pixel pitch determines the angle of the display or the power of the lenses needed to achieve a wide view angle. The space–bandwidth product, which is related to the numerical aperture of the holographic grating, determines the maximum depth range and number of resolvable views the display will possess. Finally, the optical non-idealities of the modulator give rise to noise and artefacts in the display output. Current state-of-the-art technologies for spatial light modulation (for example, liquid crystal, micro-electro-mechanical systems (MEMS)[1,2], and bulk-wave acousto-optic modulators[3]) have proven challenging to employ in holographic video displays. Before using these modulators in a holographic display, one must address their low bandwidth, low diffraction angle, quantization error, and the presence of zero order and other noise (see Fig. 1) as well as the spatial or temporal multiplexing of colour. Much of the cost and complexity of modern holographic displays is due to efforts to compensate for these deficiencies by, for example, adding eye tracking to deal with low diffraction angle[4], duplicating and phase shifting the optical path to eliminate the zero order[5], or creating large arrays of spatial light modulators to increase the display size[6]. The cost and complexity of holographic video displays could be greatly reduced if a spatial light modulator could be made to have better affordances than the liquid crystal and MEMS devices currently used.

We have developed a spatial light modulator based on anisotropic leaky-mode coupling that brings the tools of guided wave optics to bear on the challenges of holographic video and possesses many advantages over liquid crystal and MEMS devices when applied to holographic video display. Here we describe how the device can be fabricated inexpensively and made to support an aggregate temporal bandwidth of more than 50 billion pixels per second (50 Gpixels $s^{-1}$)—an order of magnitude increase over the current state-of-the-art. (A graphical representation of the modulator fabrication process can be found in Supplementary Figs 1 and 2.) We also demonstrate a threefold increase in angular deflection over other modulator technologies due to the edge-lit nature of the waveguide grating structure and the resulting increase in space–bandwidth product. The modulator exploits guided-wave phenomena, most notably anisotropic mode conversion for the elimination of zero-order light and tunable wavelength filtering for the simultaneous and superimposed modulation of colour signals.

Structurally, an anisotropic leaky-mode coupler is a proton-exchanged[7] channel waveguide on a lithium niobate substrate with a transducer at one end[8,9]. The waveguide is anisotropic and only guides light in one polarization. When excited by a radio frequency signal, the transducer generates surface acoustic waves[10] (SAWS) that propagate collinearly with the light trapped in the anisotropic waveguide (see Fig. 2a). When the phase-matching condition is met,

$$\beta_{\text{guided}} - K_{\text{grating}} = \beta_{\text{leaky}} \quad (1)$$

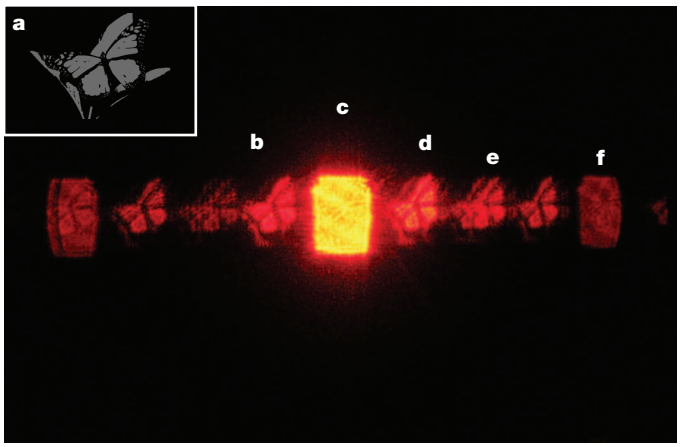


**Figure 1 | Artefacts from a holographic stereogram on a pixelated (liquid crystal on silicon) modulator.** **a**, The stereogram mask; **b**, intended output; **c**, zero order (undiffracted light); **d**, unwanted conjugate image; **e**, higher-order images and quantization noise; **f**, diffracted order arising from the modulator pixel structure. The scene used to generate this stereogram was provided by J. Buchholz.

[1]MIT Media Lab, Massachusetts Institute of Technology, Cambridge, Massachusetts 02139, USA.

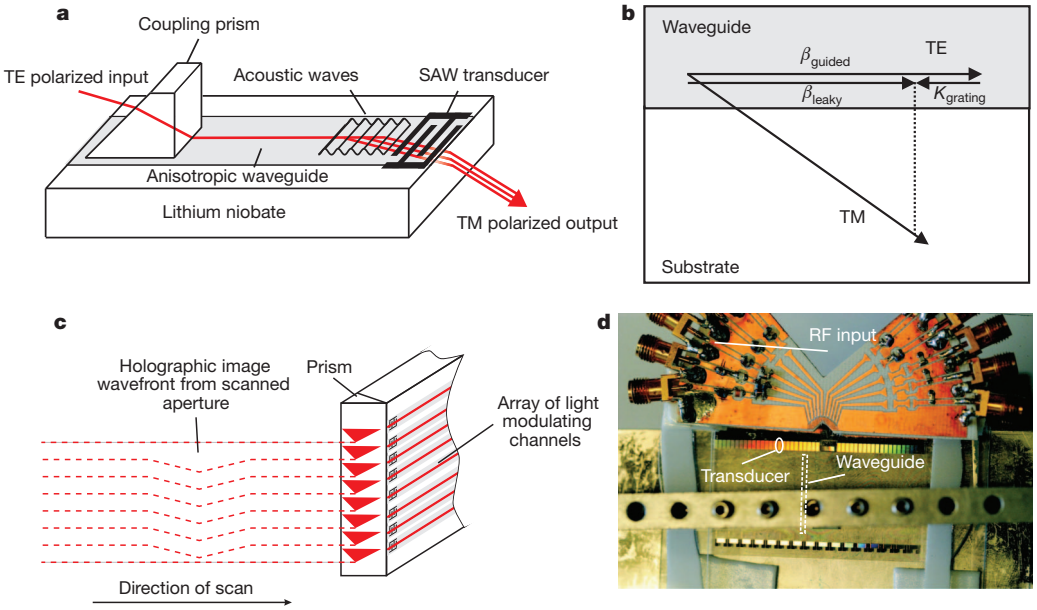


**Figure 2 | The structure and function of anisotropic mode-coupling modulators and modulator arrays.** **a**, Single channel anisotropic mode-coupling modulator. Guided, TE polarized light is converted by acoustic waves (launched from an SAW transducer) into leaky TM polarized light. The acoustic waves act as the holographic diffraction pattern. **b**, Phase matching condition for mode coupling. **c**, The holographic image is formed by scanning the aperture of the anisotropic waveguide device having one or more channels. **d**, A multichannel anisotropic waveguide modulator. The modulator pictured has more than 40 channels. Devices with as many as 1,250 channels are being fabricated.

where $\beta_{guided}$ is the wavevector of the guided TE (transverse electric) mode, $K_{grating}$ is the grating vector corresponding to the acoustic pattern encoded with holographic information, and $\beta_{leaky}$ is the component of the wavevector of the leaky TM (transverse magnetic) mode along the direction of the grating vector and the guided mode (see Fig. 2b).

The acoustic pattern, encoded with holographic information, couples the guided light into a leaky mode of orthogonal polarization which leaves the waveguide–substrate interface. The index contrast of the waveguide–air interface is much higher than that of the waveguide–substrate interface; this asymmetry of boundary conditions means that there is no conjugate image (an unwanted mirror image of the hologram output that is formed by symmetric gratings). This leaky mode emits a wavefront-modulated fan of light that leaves one face of the wafer and forms part of a holographic output image. Each channel waveguide writes one or more lines of the output, and several channels can be fabricated next to each other to create large aggregate bandwidths suitable for large display size and resolution (see Fig. 2c). Such a fabricated multichannel device is shown in Fig. 2d.

## Advantages of leaky-mode couplers

Anisotropic leaky-mode couplers possess several advantages over other spatial light modulators used for holographic video (see Table 1). In addition to being simple to fabricate and drive, they are capable of high deflection for a given spatial grating pitch and can make use of tools from guided-wave optics to address noise and colour multiplexing.

Modulators with defined pixel structure and a backplane (for example, liquid crystal and MEMS devices) become more complex as pixels are added, which constrains scalability. Bulk-wave acousto-optic modulators can produce the acoustic equivalent of 100 million pixels per second (100 Mpixels $s^{-1}$) per acoustic channel; however, channels cannot be placed too closely together because of the resulting crosstalk. Anisotropic leaky-mode couplers enjoy lateral guidance of the acoustic wave, which makes it possible for adjacent channels to be placed tens of micrometres apart and for hundreds of channels to be placed side-by-side on a single substrate, thereby providing aggregate bandwidths in excess of 50 Gpixels $s^{-1}$. This bandwidth is nearly an order of magnitude greater than the temporal bandwidth of current pixelated modulators. A device with 500 channels could provide enough bandwidth to drive a horizontal-parallax only (HPO) holographic display one metre in width. At the time of publication, we are fabricating devices with as many as 1,250 channels.

Fabrication of active liquid crystal and MEMS devices requires as many as 20 or more mask steps to define both the pixels and the associated backplane. Only two masks are required to fabricate guided-wave modulators: one to define the waveguide structure and one to pattern the transducers. The resulting fabrication and cost are similar to that of common SAW filters which sell for a dollar or less. A device capable of producing standard resolution HPO holographic video images would cost in the low tens of dollars to fabricate, as a conservative estimate.

Guided-wave modulators are analogue devices and can be driven by up-converted, standard analogue video signals, generated by, for

**Table 1 | Advantages of anisotropic waveguide modulators**

| Property | Pixelated modulator | Anisotropic waveguide modulator |
|---|---|---|
| Temporal bandwidth | 5 Gpixels $s^{-1}$ (assuming an 8 Mpixel SLM) | 50 Gpixels $s^{-1}$ (assuming a 500 channel modulator) |
| Output angle ($\lambda = 532$ nm, $\Lambda = 12$ μm) | 2.54° | 24.7° |
| Output polarization orthogonal to zero order? | No | Yes |
| Superfluous orders at output | Multiple | None |
| Fabrication complexity | 20 masks | 2 masks |
| Superfluous conjugate mode | Yes | No |
| Hologram approximation basis | Quantized pixels | Sinusoidal waves |
| Colour multiplexing | Space/time | Space/time/frequency |

Pixelated modulators considered here are MEMS and liquid crystal devices. All values are approximate. It should be noted that the angle of the output light in an anisotropic modulator is a function of waveguide parameters, such as the orientation of the substrate material (lithium niobate, *x*-cut, *y*-propagating in this case), and the wavenumber of the guided mode.

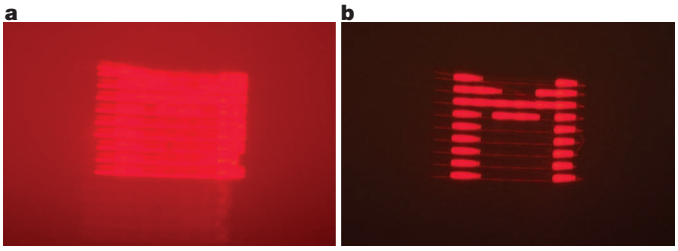


**Figure 3 | Polarization rotation to exclude noise.** **a**, **b**, The scanned output of the modulator is shown without a polarizer (**a**) and with a polarizer to exclude noise (**b**).

example, standard graphics cards commonly used in high-end graphics work. Because the modulators are analogue and have no pre-defined pixel microstructure, there is no intrinsic quantization of the signal. The device transducers can be used as filters to band-limit quantization noise that might be present in the video signal. As with pixelated modulators, light may diffract from harmonics of the acoustic signal, giving rise to higher-order diffracted signals; however, in anisotropic mode couplers, typically only one order is present at the output of the device. This is because conjugate modes are prohibited by waveguide asymmetry and higher-order modes are suppressed at the output by high angular separation of orders and total internal reflection.

In addition to the points given above, we elaborate here on three advantages of particular interest made possible by the waveguide nature of the device: hologram polarization rotation, increased angular deflection, and simultaneous and superimposed red-green-blue (RGB) modulation.

## Polarization rotation

The waveguide in the guided-wave acousto-optic modulator is anisotropic so that it supports guided modes of only one polarization; modes of the orthogonal polarization are leaky. The acoustic signal couples light from the fundamental extraordinary guided mode to the first order leaky mode, rotating its polarization along the way[11,12]. As a result, the holographic image produced by the anisotropic waveguide modulator has a polarization that is orthogonal to all of the other light in the system. This allows noise, including zero-order light, to be excluded from the output with a polarizer, as shown in Fig. 3.

## Wider angular deflection

Because the acoustic wave is being effectively illuminated by light at a glancing angle rather than at normal incidence, the resulting diffracted angle can be more than three times higher than it would be at normal incidence on another modulator of the same pixel pitch. This is shown in Fig. 4a, which was generated from the grating equation

$$\sin\theta_{out} - \sin\theta_{in} = \frac{m\lambda}{\Lambda} \quad (2)$$

where $\theta_{in}$ is the angle of the illumination light, $\theta_{out}$ is the angle of the output light, $\Lambda$ is the grating period, $\lambda$ is the wavelength of light used, and $m$ is the diffracted order. Standard modulators are illuminated near the grating normal but waveguided light interacts with the acoustic grating nearly collinearly. The differential effect of output angle with incident angle is shown in Fig. 4b. This effect is further magnified when the grating is inside a high-index material, as is the case in waveguide modulators. This is because the signal light is further deflected by refraction at the output face of the substrate. For the anisotropic modulator demonstrated here, the output angle for 532 nm light was measured to be 24.7° for a 12 μm period acoustic grating generated on the device by a 326 MHz radio-frequency signal. Because the anisotropic interaction limits the usable bandwidth of the modulator to approximately 50 MHz per colour (ref. 8), and because we use demagnification in our supporting optics to choose the final display view angle, only a fraction (2.6° for 532 nm light) of this angular extent is used. The modulator will present an output that, when scanned, looks like a 1 m image with a 2.6° view-zone. This image will be demagnified for a final display output with approximately 10 cm of extent and a 26° view-zone. Having a small input angle and large demagnification ratio is intentional in our display, as it reduces the requirements placed on the scanning optics and keeps the display compact. In our display geometry, the chief advantage of this angular expansion in anisotropic devices is that it gives approximately a fivefold increase in the rate of angular deflection (degrees of deflection per MHz of signal bandwidth) than is typically available to lithium niobate acousto-optic deflectors, bringing the angular rate of deflection of the anisotropic modulator almost to parity with slow shear mode tellurium dioxide Bragg cells but at a fraction of the cost and with the added advantages of lower acoustic attenuation and dramatically higher channel capacity.

## Simultaneous, superimposed RGB modulation

Anisotropic waveguide devices are capable of multiplexing colour in frequency rather than in time or space. In liquid crystal, MEMS and bulk wave acousto-optic modulators, it is necessary either to dedicate pixels to one colour or to illuminate the SLM sequentially, thereby reducing the resolution or the maximum refresh rate. However, waveguide devices can use wavelength division multiplexing, which allows

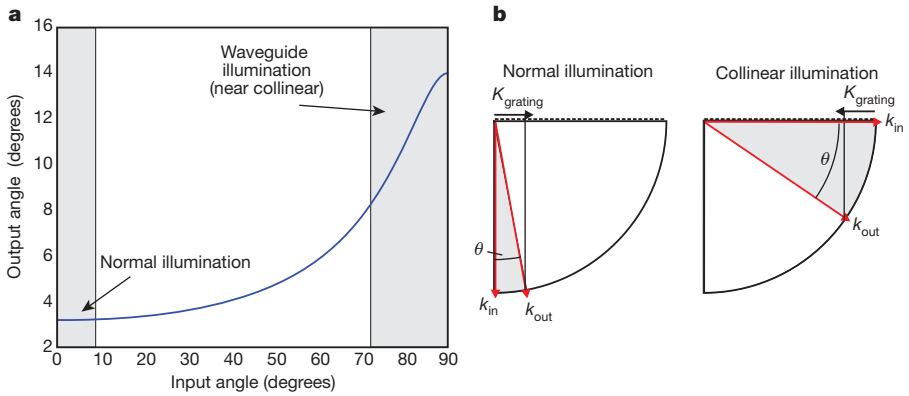


**Figure 4 | Waveguide illumination for larger angular diffraction.** **a**, Diffraction output angle versus input illumination angle for a 10 μm period grating illuminated with 633 nm light. Pixelated modulators are illuminated at angles near the perpendicular (these near-perpendicular angles are indicated by the left-most grey region), which affords a smaller range of diffracted output angles than is possible for a device illuminated at nearly collinear angles (near-collinear angles are indicated by the right-most grey region) as is the case in our anisotropic waveguide modulator. **b**, Angular output magnification for near-collinear waveguide illumination (right) relative to illumination at normal incidence (left) where $k_{in}$ is the momentum vector of the input light (the illumination), $k_{out}$ is the momentum vector of the diffracted output light, $\theta$ is the diffraction angle (highlighted by grey regions) and $K_{grating}$ is the momentum vector of the grating. Note that $\theta$ is much larger for collinear illumination even though $K_{grating}$ is the same in both cases.

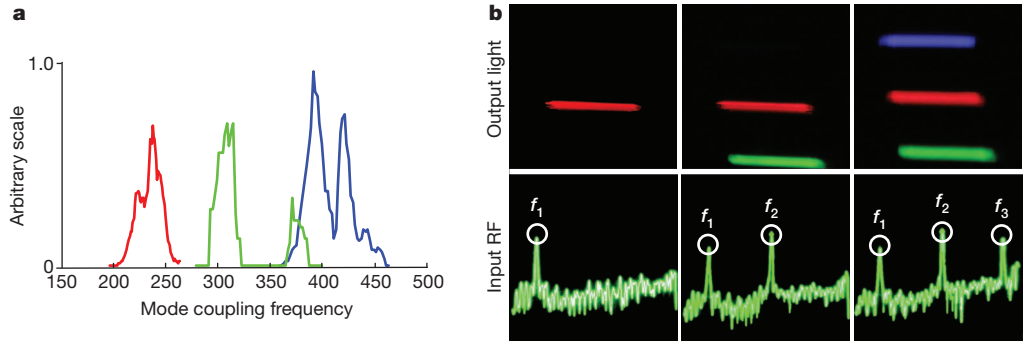


**Figure 5 | Wavelength division multiplexing for colour displays.** **a**, Frequency response of the anisotropic mode coupling device for red, green and blue light. **b**, Frequency multiplexing of red, green and blue light. The left panels show red output light for a low frequency input, $f_1$. The middle panels show both red and green output for an input containing both low frequency, $f_1$, and middle frequency, $f_2$, information. The right panels show red, green and blue outputs for an input signal containing low, medium and high frequencies ($f_1$, $f_2$ and $f_3$ respectively).

for simultaneous and superimposed modulation of red, green and blue light, so no colour filter wheel or separation of red, green and blue channels is necessary. This effect arises because the phase matching condition is wavelength-dependent. Red light mode converts at a lower frequency than green light, which in turn couples at a lower frequency than blue, allowing one to choose which colour to modulate by 'colouring' the frequency spectrum of the electrical signal sent to the modulator's transducers (see Fig. 5a). Because each channel is essentially a white-light emitter, the illumination of the device becomes trivial. Each channel or group of channels can be flood-illuminated by continuous red, green and blue light sources. This interaction is particularly well suited for colour holographic displays because the phenomenon of leaky mode coupling allows enough bandwidth for each colour to scan out a useful fan of angles but at the same time each passband is sufficiently separated to allow for independent operation. Additionally, it is also very convenient that all three colour bands fit approximately within the 200 MHz available from analogue video outputs of standard graphics processors.

To demonstrate simultaneous, superimposed RGB modulation, we illuminated one channel of an anisotropic waveguide array with continuous red, green and blue light ($\lambda = 633$ nm, $\lambda = 532$ nm, and $\lambda = 445$ nm). We stimulated a single, wideband transducer with a radio-frequency signal containing colour information that was separated in frequency with red information centred at 213 MHz, green at 333 MHz and blue at 387 MHz. The diffracted output of the modulator was scanned with $x$–$y$ galvanometric mirrors to generate the test pattern in Fig. 5b. Then the output of the modulator was de-scanned with a rotating polygon and multiplexed vertically with a galvanometer to generate the holographic stereogram images (see Fig. 6) using a modified Scophony architecture[3,13] (see Fig. 7). The holographic stereograms were displayed at a resolution of 156 pixels $\times$ 177,600 pixels and at a refresh rate of 5 frames $s^{-1}$ (here frame rate was traded for vertical resolution so an image could be made from a single channel device).

## Other modulator parameters

Other parameters important to spatial light modulators are diffraction efficiency, temporal bandwidth, space–bandwidth product and cost. Our devices have had a wide range of efficiencies, all less than 10% for 0.5 W of applied radio-frequency power. Several other researchers, with more optimized designs (better-quality waveguides, narrower channels and carefully tuned annealing times), have reported efficiencies up to 90% (for 0.58 W of applied power) with room for additional improvement[14–16]. The 3 db bandwidth per channel of the device used here has been measured to be approximately 40 MHz per colour when using a uniform transducer(see Fig. 5a) and approximately 60 MHz when using a chirped transducer. This is consistent with the literature[8]. Given an acoustic wave speed of approximately 3,700 m $s^{-1}$ and taking 50 MHz as the channel bandwidth, the space–bandwidth product of the device aperture is 13.5 cycles per millimetre of interaction length. The interaction length can be as great as 50 mm if limited only by acoustic attenuation. The maximum number of cycles in the scanned aperture of a 30 Hz display is 1.67 Mpixels per channel per frame. The device used here, fabricated as part of a two-wafer run which included electron-beam lithography, cost approximately US$50 to process at MIT's fabrication facilities. By processing 10 wafers at a time and by using photolithography, rather than electron-beam direct writing to define the transducers, the same device could be fabricated for less than US$3. Furthermore, an inexpensive geometry suitable for housing this device has been described[17].

## Considerations for displays

Given the advantages described here, a new family of flexible holographic video displays is now possible. In holographic video displays using anisotropic mode couplers, the output of the device is scanned to create large outputs by persistence of vision. Because the modulator is an analogue device, display parameters such as frame rate, view angle, image extent and vertical resolution can be interchanged fluidly as long as the bandwidth budget is satisfied. If more space–bandwidth product (which is related to the concept of numerical aperture and to the total number of scannable points in diffractive systems) is needed, the length of the channels can be extended to provide longer interaction lengths in accordance with the expression $N = L(\Delta f/v)$, where $N$ is the space–bandwidth product (or number of scannable points), $L$ is the channel length, $v$ is the velocity of the acoustic wave and $\Delta f$ is the bandwidth of the anisotropic mode coupling interaction. If more temporal bandwidth is needed, more channels can be added to the

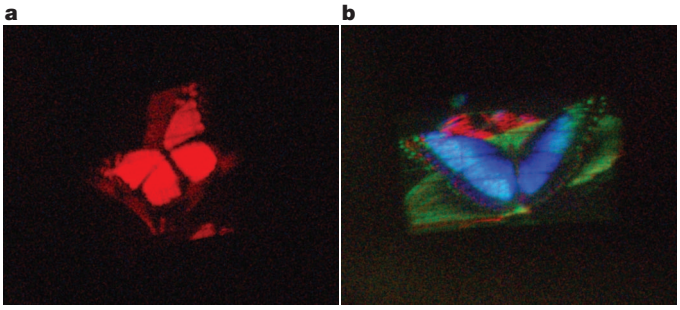


**Figure 6 | Holographic stereograms made with a single channel anisotropic waveguide modulator, measuring 35 mm by 20 mm at the output of the display.** **a**, Monochrome holographic stereogram. **b**, Colour holographic stereogram using simultaneous and superimposed modulation of red, green and blue light. The scene used to generate the stereogram in **a** was provided by J. Buchholz; Neil Doren Photography provided the live scene used to generate the holographic stereogram in **b**.

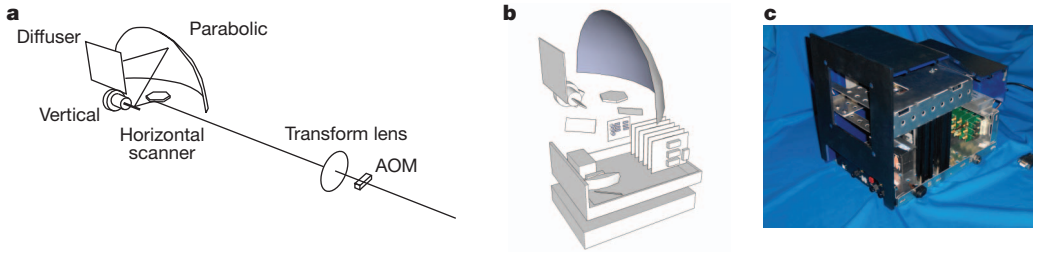


**Figure 7 | PC-driven holographic video monitor.** **a**, Holographic video monitor optical path containing a modulator, transform lens, horizontal polygon scanner, vertical galvanometric scanner, parabolic output lens and diffuser. **b**, Internal path folding of holographic video monitor. **c**, Assembled holographic video monitor.

modulator. When there are enough channels in an array to write all the necessary output lines simultaneously, there is no longer a need for vertical scanning and the problem of holographic video display becomes reduced to a single axis scan. With all lines written at once, the scanning optics are only required to make a full sweep once every 1/30th or 1/60th of a second, greatly expanding the size and type of scanning elements that may be used, which, interestingly, means that large displays can be more physically parsimonious than small ones.

Having demonstrated the advantages of anisotropic mode couplers, we are now exploring displays based on arrays of these devices such as a small, PC-driven, holographic video monitor and large-scale displays exceeding half a metre in width driven by dedicated hardware. Given the recent progress made in using graphics processing units (GPUs) for hologram fringe computation[18–20], it is now possible, using anisotropic mode coupling arrays driven by a commodity PC with a bank of high-end graphics cards, to make holographic video monitors with full-colour, standard video resolution and a 30 Hz refresh rate. Our research shows such a monitor might be constructed for less than US$500 (not including light sources). We are also investigating dedicated hardware solutions for driving large displays requiring tens of gigapixels per second.

## METHODS SUMMARY

The modulators used here were fabricated from wafers of *x*-cut lithium niobate. The waveguides were formed by annealed proton exchange. The waveguides were defined by contact lithography. The transducers were defined by either contact lithography or direct electron-beam writing. The devices were impedance matched with lumped L-networks. Light was coupled into the waveguides using a rutile prism. The holographic stereogram images were created by taking one stereogram view at a resolution of 296 pixels × 156 pixels, stretching its resolution to 29,600 pixels × 156 pixels, and finally stitching 12 of these images together for a composite resolution of 355,200 pixels × 156 pixels. The α values of each of the red, green and blue channels of this image were multiplied by a different sinusoidal pattern in an OpenGL shader. All three colour signals were summed and divided by three, and sent out one of the video card outputs (for example, the nominal 'red' channel). This signal was then up-converted and amplified before entering a single transducer of the modulator array. Light from three lasers (at $\lambda = 445$ nm, $\lambda = 532$ nm and $\lambda = 633$ nm) was combined in an X cube and focused with an achromatic lens into one channel of an anisotropic leaky-mode coupling array. The output of the device was spatially filtered and focused on to the face of a spinning polygon (to optically descan the holographic fringe pattern so that it would appear stationary), vertically scanned onto a parabolic mirror (using the geometry shown in Fig. 7a), and finally imaged by a camera. For simplicity, only the view entering the camera was computed and displayed. The vertical diffuser shown in Fig. 6a, which extends the vertical viewzone of HPO holograms, was not used. A graphical representation of the modulator fabrication process can be found in Supplementary Figs 1 and 2.

**Full Methods** and any associated references are available in the online version of the paper.

**Received 30 November 2012; accepted 23 April 2013.**

1. Kreis, T., Aswendt, P. & Hofling, R. Hologram reconstruction using a digital micromirror device. *Opt. Eng.* **40,** 926–933 (2001).
2. Pearson, E. *MEMS Spatial Light Modulator for Holographic Displays*. Masters thesis, Massachusetts Institute of Technology (2001).
3. Hilaire, P., Benton, S. & Lucente, M. Synthetic aperture holography: a novel approach to three-dimensional displays. *J. Opt. Soc. Am. A* **9,** 1969–1977 (1992).
4. Häussler, R., Schwerdtner, A. & Leister, N. Large holographic displays as an alternative to stereoscopic displays. *Proc. SPIE Stereosc. Displays Applicat.* **XIX,** 68030M (2008).
5. Chen, G.-L., Lin, C.-Y., Kuo, M.-K. & Chang, C.-C. Numerical suppression of zero-order image in digital holography. *Opt. Express* **15,** 8851–8856 (2007).
6. Sato, K., Sugita, A., Morimoto, M. & Fujii, K. Reconstruction of color images at high quality by a holographic display. *Proc. SPIE Practical Hologr.* **XX,** 6136 (2006).
7. Jackel, J., Rice, C. & Veselka, J. Proton exchange for high-index waveguides in $LiNbO_3$. *Appl. Phys. Lett.* **41,** 607–608 (1982).
8. Matteo, A., Tsai, C. & Do, N. Collinear guided wave to leaky wave acoustooptic interactions in proton-exchanged $LiNbO_3$ waveguides. *IEEE Trans. Ultrason. Ferroelectr. Freq. Control* **47,** 16–28 (2000).
9. Rust, U. & Strake, E. Acoustooptical coupling of guided to substrate modes in planar proton-exchanged $LiNbO_3$-waveguides. *Proc. Integrated Photonics Research* ME4 (Vol. 10 OSA Technical Digest Series, Optical Society of America, 1992).
10. Onural, L., Bozdagi, G. & Atalar, A. A new holographic 3-dimensional television display. *Proc. 1991 IEEE Ultrason. Symp.* **1,** 543–546 (1991).
11. Proklov, V. & Korablev, E. Multichannel waveguide devices using collinear acoustooptic interaction. *Proc. 1992 IEEE Ultrason. Symp.* **1,** 173–178 (1992).
12. Ito, K. & Kawamoto, K. An optical deflector using collinear acoustooptic coupling fabricated on proton-exchanged $LiNbO_3$. *Jpn. J. Appl. Phys.* **37,** 4858–4865 (1998).
13. Lee, H. The scophony television receiver. *Nature* **142,** 59–62 (1938).
14. Do, N. T., Su, J., Yoo, J., Matteo, A. M. & Tsai, C. S. High-efficiency acoustooptic guided-mode to leaky-mode conversion in proton-exchanged lithium niobate waveguides. *Proc. 1999 Ultrason. Symp.* 613–616 (1999).
15. Ohmachi, Y. & Noda, J. $LiNbO_3$ TE-TM mode converter using collinear acoustooptic interaction. *IEEE J. Quantum Electron.* **13,** 43–46 (1977).
16. Sohler, W. Integrated optics in $LiNbO_3$. *Thin Solid Films* **175,** 191–200 (1989).
17. Smalley, D. *et al.* Holovideo for everyone: a low-cost holovideo monitor. *J. Phys. Conf. Ser.* **415,** 012055 (2013).
18. Bove, V., Plesniak, W., Quentmeyer, T. & Barabas, J. Real-time holographic video images with commodity PC hardware. *Proc. SPIE Stereosc. Displays Applicat.* **XII,** 255262 (2005).
19. Barabas, J., Smithwick, Q., Smalley, D. & Bove, V. M. Real-time shader rendering of holographic stereograms. *Proc. SPIE Practical Hologr.* **XXIII,** 723303 (2009).
20. Smithwick, Q., Barabas, J., Smalley, D. & Bove, V. M. Interactive holographic stereograms with accommodation cues. *Proc. SPIE Practical Hologr.* **XXIV,** 761903 (2010).

**Supplementary Information** is available in the online version of the paper.

**Acknowledgements** This work was supported by consortium funding at the MIT Media Lab and by Intel Corp. Graphics hardware was provided by NVIDIA. D.E.S. thanks the MIT Nanostructures Laboratory for use of its facilities, E. Pearson for discussion, and D. Novy for assistance with GPU coding.

**Author Contributions** D.E.S. performed experimental work and fabricated devices. D.E.S., Q.Y.J.S. and V.M.B. participated in conceptualization of waveguide phenomena for holographic video. D.E.S., Q.Y.J.S., V.M.B., J.B. and S.J. participated in the design and evaluation of experiments.

**Author Information** Reprints and permissions information is available at www.nature.com/reprints. The authors declare no competing financial interests. Readers are welcome to comment on the online version of the paper. Correspondence and requests for materials should be addressed to D.E.S. (desmalley@gmail.com).

## METHODS

**Proton-exchanged waveguide.** The proton-exchange process is illustrated in Supplementary Fig. 1. An *x*-cut lithium niobate wafer 1 mm thick was cleaned using a standard cleaning process (3:1:1 ammonium hydroxide, hydrogen peroxide and water heated to 80 °C), rinsed in deionized water and then with a solvent such as isopropanol (IPA) to prevent residue formation during drying. Physically enhanced chemical vapour deposition (PECVD) was used to deposit a 200 nm silicon dioxide layer on the wafer. Negative resist (Futurrex NR8-1000) was spun on at 3,000 r.p.m. and the wafer was pre-baked in an oven at 100 °C for 7 min. The pattern was exposed with a light-field mask to define the waveguides, the resist was developed in 2% tetramethylammonium hydroxide (TMAH) solution and the underlying silicon dioxide etched in a buffered oxide etch for 30 s. Resist was removed with acetone. Benzoic acid was heated to 238 °C (it is recommended that the melt be diluted with 1% lithium benzoate by weight, but this was not done for the present work) and the wafer carefully placed in the melt for 34 min. (Experience shows that the wafer must be warmed gradually before entering the melt or it may break; lowering it to just above the melt surface allows it to warm to the melt temperature.) The wafer was removed carefully and slowly, to avoid cracking, cooled and cleaned with acetone and IPA. Silicon dioxide was removed by submerging the wafer in buffered oxide etch for 30 s, then the wafer was placed in a covered quartz dish and baked for 45 min in an oven preheated to 375 °C.

**Al transducers.** The lift-off process is illustrated in Supplementary Fig. 2. On a clean proton exchanged substrate, 600 nm of poly(methyl methacrylate) (PMMA) was spun, then the substrate was baked at 150 °C for 15 min. A layer of E-spacer (Showa Denko) or Aquasave (Mitsubishi Rayon) was then spun on to prevent charging while direct writing with an electron beam (we note that this could also be accomplished with a 20-nm-thick evaporated layer of chrome which would have to be stripped before development, but this was not done for the present work). An electron beam was used to direct write the transducer pattern at a dose of approximately 250 $\mu C\,cm^{-2}$. For the device used in this paper, the transducer was the composed of three regions each with a uniform period corresponding to 270 MHz, 310 MHz and 380 MHz. (These frequencies will vary with proton exchange time and temperature. Also, note that the features of these transducers are large enough to be patterned by photolithography if desired, but electron beam direct write allows for a high degree of customization and is convenient for small samples.) The Aquasave or E-spacer was removed from the exposed sample with deionized water, and the PMMA developed in a 1:1 mixture of IPA:MIBK (methyl isobutyl ketone) for approximately 30 s. A 200 nm film of aluminium was deposited by e-beam evaporation, and the sample placed in *N*-methyl-2-pyrrolidone (NMP) heated to 50 °C, and left until the Al lifted off. (Sonication at low power for 5 s may be required.) The exit face of the sample was polished down to a 0.3 μm grit, and the sample cleaned with acetone, methanol and isopropyl alcohol. The transducers were wire-bonded, using 2 thousandths of an inch thick aluminium wire, to a copper PCB board equipped with a 50 Ω radio-frequency connector. Impedance matching for the highest resonance was achieved with a lumped element L network (typically our samples required a 100 nH series inductor followed by a 9 pF shunt capacitor); matching the highest resonance was done to make up for the fact that the blue interaction is the least efficient.

**Experiments.** Polarization rotation. To demonstrate polarization rotation, light from a diode laser at $\lambda = 633$ nm was evanescently coupled into an anisotropic leaky mode device using a rutile prism. The output of the device was scanned with a *x*–*y* scanner onto a camera sensor (a camera with the lens removed) to allow for lower ISO images and less camera noise. A polarizer was placed at the output of device.

Frequency multiplexing of colour. The mode coupling frequency response for red, green and blue light was measured by coupling laser light into the $TE_1$ guided mode of the device and then exciting an acoustic wave with a radio-frequency signal which swept from 150 to 500 MHz. The light that was coupled into the leaky mode was measured with a light meter. This process was repeated for red, green and blue. Note that the shape of the device's frequency response represents not only the frequency response of the anisotropic interaction alone but also the response of the SAW transducer and the impedance matching network which was designed to give the best match at frequencies responsible for blue mode coupling. The power of the input light was 10 mW for red and 100 mW for green and blue. Holographic stereograms. The holographic stereogram images were created by taking one stereogram view at a resolution of 296 pixels× 156 pixels, stretching its resolution to 29,600 pixels × 156 pixels, and finally stitching 12 of these images together for a composite resolution of 355,200 pixels × 156 pixels. The α values of each of the red, green and blue channels of this image were multiplied by a different sinusoidal pattern in an OpenGL shader. All three colour signals were summed and divided by three, and sent out via one of the video card outputs (for example, the nominal 'red' channel). This signal was then up-converted and amplified before entering a single transducer of the modulator array.

For holographic stereogram images, light from three lasers (at $\lambda = 445$ nm, $\lambda = 532$ nm and $\lambda = 633$ nm) was combined in an X cube and focused with an achromatic lens into one channel of an anisotropic leaky mode coupling array. The output of the device was spatially filtered and focused on to the face of a spinning polygon (to optically descan the holographic fringe pattern so that it would appear stationary), vertically scanned onto a parabolic mirror, and finally imaged by a camera. For simplicity, only the view entering the camera was computed and displayed. The vertical diffuser, which extends the vertical viewzone of HPO holograms, was not used.